Observation and analysis of the hyperfine structure of near-dissociation levels of the NaCs $c\,^3\Sigma^+$ state below the dissociation limit $3S_{1/2} + 6P_{3/2}$

Wenliang Liu,[1] Jizhou Wu,[1] Jie Ma,[1,2,*] Peng Li,[1] Vladimir B. Sovkov,[1,3,*] Liantuan Xiao,[1,2] and Suotang Jia[1,2]

[1]*State Key Laboratory of Quantum Optics and Quantum Optics Devices, Institute of Laser Spectroscopy, College of Physics and Electronics Engineering, Shanxi University, Taiyuan 030006, People's Republic of China*

[2]*Collaborative Innovation Center of Extreme Optics, Shanxi University, Taiyuan, Shanxi 030006, People's Republic of China*

[3]*St. Petersburg State University, 7/9 Universitetskaya Nab., St. Petersburg 199034, Russia*

(Received 20 July 2016; revised manuscript received 29 August 2016; published 30 September 2016)

We report photoassociation (PA) of ultracold Na and Cs atoms in a dual-species magneto-optical trap. Trap loss spectroscopy of the ultracold polar NaCs molecules formed by PA, which carries information about relative PA transition strengths, has been experimentally obtained by using highly sensitive modulation spectroscopy technique. The fine and hyperfine effects at near-dissociation levels of NaCs molecular $c\,^3\Sigma^+$ state are observed and modeled. The interaction Hamiltonian is described in terms of the Hund's case (a) coupling scheme. The molecular hyperfine structure of near-dissociation levels is simulated within a simplified model of four interacting vibrational levels belonging to different initially unperturbed electronic states. The results of the simulation infer that the interaction parameters of the observed near-dissociation levels are close to the asymptotic parameters of the pair of atoms. The coupling of the electronic states is essential for forming the hyperfine structure.

DOI: 10.1103/PhysRevA.94.032518

I. INTRODUCTION

Much attention has been paid to the study of cold and ultracold molecules over the last decade [1–3]. Ultracold polar molecules are of particular interest because their intrinsic permanent electric dipole moments (EDM) allow them to interact strongly in the presence of electric fields. In addition, the dipole-dipole intermolecular interactions are long range, anisotropic, and tunable. The properties, combined with the exquisite control of ultracold systems such as the ones trapped in the electronic trap [4], offer exciting prospects in the field of quantum controlled chemistry [5,6], precision measurements [7–9], quantum computations [10], and quantum simulations [11,12]. Various methods to produce ultracold polar molecules have been proposed [13]. Photoassociation (PA) of ultracold atoms is one of the most efficient techniques. Ultracold polar molecules have been produced by PA in LiCs, LiRb, KRb, RbCs, LiK, and YbRb [14–19]. PA not only serves as a significant approach for preparing ultracold molecules at low temperatures in the micro-Kelvin range, but also gives rise to a new high-resolution molecular spectroscopic technique, i.e., PA spectroscopy. This spectroscopy is a unique tool to detect the molecular long-range states, which has provided a wealth of information about molecular structures in the near-dissociation region [20]. In addition, it has been widely applied in precise measurement of s-wave scattering length [21] and fundamental physical constants [22].

The NaCs molecule is a promising candidate for ultracold polar molecular experiments for many reasons. First, the rovibrational ground state of the NaCs molecule is predicted to have a large EDM of 4.6 Debye [23], which is second only to LiCs among the diatomic alkali heteronuclear molecules. Second, thanks to the efficient free-bound excitation characteristic, the one-step PA experiment can fortuitously generate large numbers of ultracold NaCs molecules in the absolute vibrational ground state [24]. Last, the NaCs molecules can be electrostatically confined using an inexpensive and easily constructed trap [4].

Bigelow and co-workers reported for the first time the formation of ultracold polar NaCs molecules via a PA experiment in 2004 [25]. In their following studies [24,26–28], PA spectroscopy of the different electronic states of NaCs molecules had been obtained using ionization detection technique and ground-state molecules had been obtained by optical pumping approaches. The ionization detection technique has the advantages of sensitivity and zero background; however, it does not provide the information about PA transition intensities due to the intervention of the extra ionization laser [29]. A feasible technique is the trap loss detection by directly monitoring the fluorescence yield from trapped atoms [30]. One of the strengths of the trap loss is that it not only provides frequency positions of PA resonances, but it also carries information about relative transition strengths, information that is not always available with other techniques such as ionization [31] but is important for studying the PA process and optimizing the energy schemes in future experiments. However, the trap loss spectroscopy of the NaCs molecules has not been previously reported, because the sensitivity of the trap loss detection is not sufficiently high while the Franck-Condon factor of a PA transition is rather small for heteronuclear molecules [32]. The trap loss spectroscopies had been obtained in some other polar molecules, such as RbCs, LiCs, LiRb, and LiK [14,15,17,18]. However, these studies are limited to observing the PA phenomenon and preparing ground-state molecules only. Detailed analysis of the trap loss spectroscopy, especially the molecular hyperfine structure in these spectra, is required for many potential applications of ultracold polar molecules, such as precision measurements and quantum simulations.

The primary purposes of the present article are: (1) to show that the trap loss technique in place of the ion detection method can be successfully used to study the ultracold heteronuclear NaCs molecule and to report the first experimental results obtained with this approach; and (2) to present a theoretical

*Corresponding authors: mj@sxu.edu.cn; vladimir_sovkov@mail.ru

model along with numerical simulations of the hyperfine structure at the NaCs near-dissociation levels observed in such experiments.

In this article, we report the trap loss spectroscopy of ultracold polar NaCs molecules induced by the PA of ultracold Na and Cs atoms using the modulation spectroscopy technique [33]. Some hyperfine structures of high-lying vibrational levels have been observed and analyzed in the $c\,^3\Sigma^+_{\Omega=1}$ electronic state. The hyperfine structure spectra containing the information on both PA resonance positions and transition intensities are simulated using a developed model that is simple but able to reproduce the overall characteristic hyperfine structure of the experimental spectra.

This article is organized as follows. In Sec. II we present the experimental setup and the experimental results, and in Sec. III we report the theoretical model. The numerical simulations are given in Sec. IV, the discussion is given in Sec. V, and the conclusions are presented in Sec. VI.

II. EXPERIMENT

Our experiment begins with overlapping dark-spot magneto-optical traps (dark-SPOT MOTs) of sodium and cesium. The dark-SPOT MOTs allow us to obtain a large number of ultracold atoms with minimal losses from light-assisted interspecies collisions [34]. The details of the apparatus are shown schematically in Fig. 1. The ^{133}Cs dark-SPOT MOT typically contains $N_{\rm Cs} \approx 6\times10^7$ of the Cs atoms at a density of 1.5×10^9 cm^{-3}, with a majority of the ^{133}Cs atoms in the lower hyperfine ($f=3$) levels of the $6s\,^2S_{1/2}$ state. The ^{23}Na dark-SPOT MOT typically contains $N_{\rm Na}\approx 9\times10^6$ of the Na atoms at a density of 2.0×10^9cm^{-3}, with a majority of the Na atoms in the lower ($f=1$) hyperfine levels of the $3s\,^2S_{1/2}$ state. The temperature of the ultracold Cs (Na) atomic sample is measured to be $\sim$120 μK ($\sim$150 μK) by using a time-of-flight method.

The PA laser is provided by a widely tunable continuous-wave Ti:sapphire laser system (Coherent MBR 110, power $\sim$3.5 W, linewidth $\sim$100 kHz). The long time frequency drift is suppressed within 500 kHz by locking to its self-reference cavity. The absolute frequency of the PA laser is measured by a wavelength meter (High Finesse-Angstrom WS/U) with an accuracy of 30 MHz. The wavelength meter is repeatedly calibrated with the Cs atomic hyperfine resonance transition, $6S_{1/2}(f=4)\longrightarrow 6P_{3/2}(f=5)$, corresponding to the wave number of 117 32.176 cm^{-1}. The PA laser beam is collimated to a $1/e^2$ diameter of 0.78 mm with a maximum available average intensity of $\sim$750 W/cm^2.

One of the simplest techniques for detecting a PA transition is to monitor the number of atoms remaining in a MOT. This number is a balance between the loading and losses. The PA of atoms introduces an additional loss mechanism: the excited molecules formed by a PA quickly decay by spontaneous emissions to hot atoms that are not recaptured by the trap or to stable molecules that are not trapped. A convenient way to monitor the number of trapped atoms in a MOT is by observing the level of the fluorescence emitted by the atoms as they are continuously bathed in the near-resonant light which forms the MOT. The variation of the atom number with the PA laser frequency gives the spectral information [31]. In our experiments, the fluorescence from the Cs (Na) dark-SPOT MOT is collected using a lens and detected by an avalanche photodiode (a photomultiplier) with a 852-nm (589-nm) bandpass filter. The direct fluorescence detection is usually not satisfying because a noise arising from stray fluorescence nearly submerges the useful signal. The lock-in method, based on modulating the fluorescence of the ultracold atom, is used to improve the detection sensitivity of the trap loss spectroscopy in our experiment [33]. A modulation frequency of 3.4 kHz (3.2 kHz) for the fluorescence from trapped Cs (Na) atoms is also used in stabilizing the trapping laser frequency. The modulated fluorescence is demodulated with a lock-in amplifier (Stanford Research SR830) and recorded by a computer.

We experimentally study the PA resonance below the Na($3S_{1/2}$) + Cs($6P_{3/2}$) asymptote, i.e., near the D_2 line of Cs at 852 nm. Figure 2 demonstrates the time evolution of the fluorescence from Na and Cs atoms corresponding to the MOT on or off, which are characterized by loading times of $t_{\rm Na}=3.3$ s and $t_{\rm Cs}=3.9$ s, respectively. Accordingly, the PA laser scanning rate is set 5 MHz/s so that the PA spectra can be observed with a reasonable resolution. It is

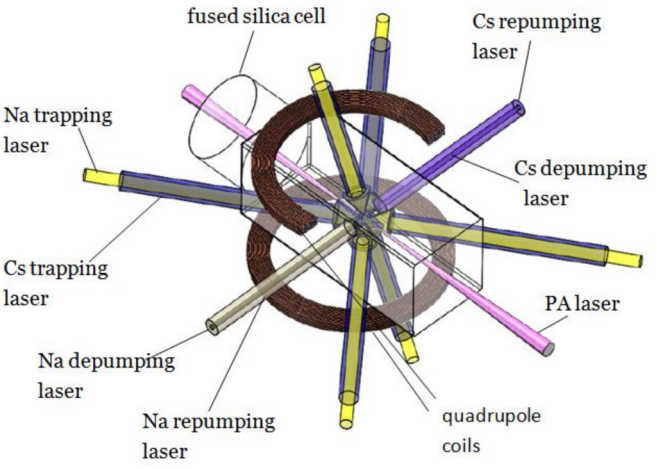

FIG. 1. Experimental setup. Simplified diagram of key elements of the apparatus. The Na and Cs ultracold atom samples are trapped in a dual-species MOT.

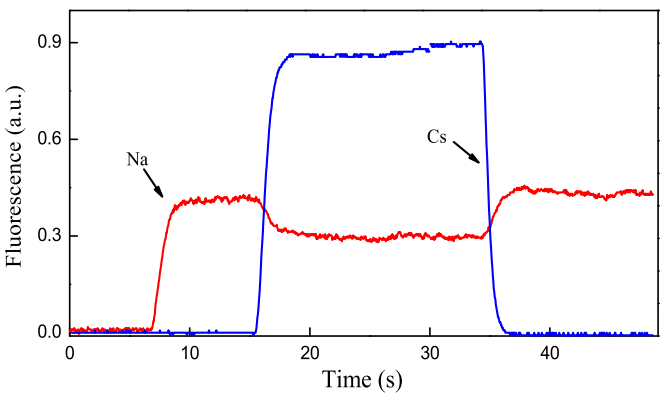

FIG. 2. Typical loading sequence of the Na+Cs dual MOT. Trapping of Na (red curve) and Cs (blue curve) is controlled by switching the corresponding repumping beam off or on.

clear from Fig. 2 that the Na atom's loss as the Cs MOT is on. So a Cs_2 PA resonance, i.e., the loss of the cesium atoms, may increase the number of the Na atoms; therefore the Na fluorescence may increase. A PA resonance leads to the formation of ultracold polar NaCs molecules in an excited electronic state and the losses of both the trapped Na and Cs atoms. The losses of the trapped Na atoms, experimentally monitored by detecting the Na atomic fluorescence signal, can represent a real PA for heteronuclear NaCs molecules, whereas the losses of the trapped Cs atoms represent the sum of PA for heteronuclear (NaCs) and homonuclear (Cs_2) molecules. Moreover, the PA-induced loss of the Cs atomic fluorescence, monitored simultaneously with the Na atomic fluorescence in the process of photoassociation in our experiment, is not distinguishable. The main reason may be that the loss of the Cs atoms caused by the formation of the heteronuclear NaCs molecules is not heavy enough to affect the total Cs atomic fluorescence. Here, we experimentally demonstrate the trap loss spectroscopy of ultracold polar NaCs molecules by detecting the Na atomic signal. As shown in Fig. 3, five typical trap loss spectra have been observed for the different rovibrational levels, whose detunings below the $(3S_{1/2}) + (6P_{3/2})$ dissociation limit are $\sim$31.7 cm^{-1}, $\sim$25.2 cm^{-1}, $\sim$14.8 cm^{-1}, $\sim$10.8 cm^{-1}, and $\sim$ 7.7 cm^{-1}, respectively. The maximum loss ratio of signal is up to 0.45. We have observed some other rotational levels ($J > 1$) and vibrational series, but the loss ratio of the signal is not satisfactory; most resonance lines are nearly indistinguishable. In order to keep the data relatively complete and organized, we do not list the other resonance lines in the manuscript.

It is worth noting that the rich hyperfine structure is observed with the available information about relative transition strengths in a PA process. Referring to the expected spectral features and the ion spectra reported in the PhD thesis [35], these spectra are assigned to five vibrational levels of $v = 61,62,64,65$, and 66 with the same lowest rotational quantum number ($J = 1$) in the $c\,^3\Sigma^+_{\Omega=1}$ electronic state.

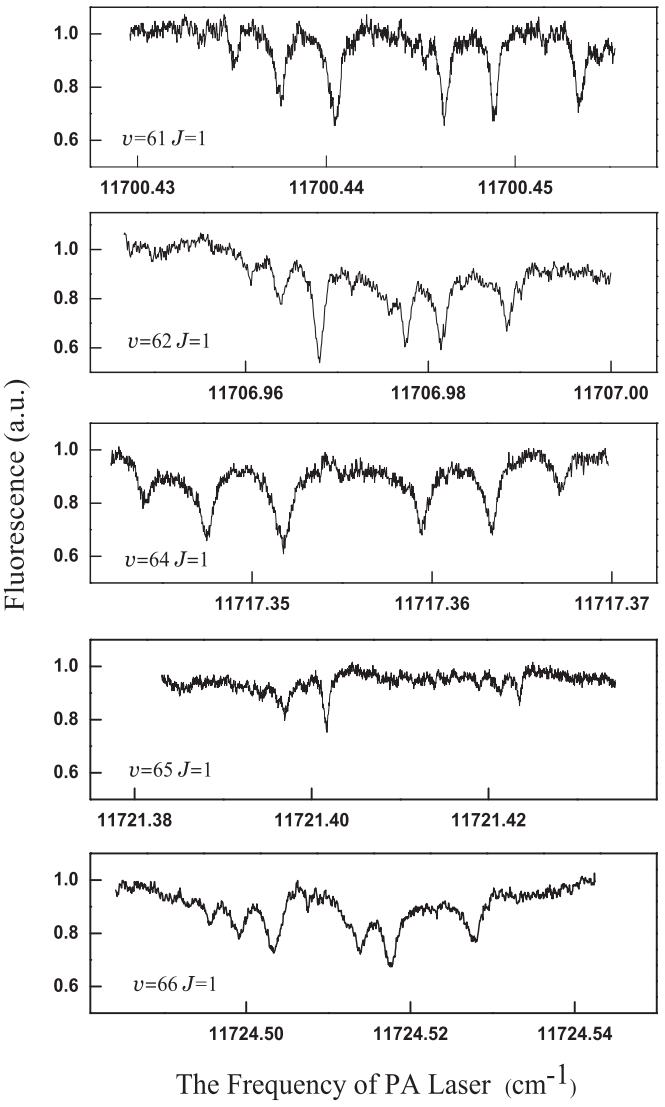

FIG. 3. Trap loss spectroscopy of $c\,^3\Sigma^+_{\Omega=1}$ electronic state. Each scan shows the resolved hyperfine structure of a single rotational level ($J = 1$) for five different vibrational levels.

III. THEORETICAL MODEL

We consider a simplified model of initially unperturbed levels belonging to one of the electronic states of the corresponding dissociation limit: $^1\Sigma^+$ and $^3\Sigma^+$ for the limit $s + s$; $^1\Sigma^+$, $^3\Sigma^+$, $^1\Pi$, $^3\Pi$, for the limit $s + p$, etc. These levels are split into a multitude of rotational, fine, and hyperfine sublevels by rotational and interaction Hamiltonians.

For the rotational Hamiltonian we used

$$H^R = \frac{\hbar^2}{2mr^2}\boldsymbol{R}^2 = B_v\big[\big(\boldsymbol{J}^2 - \boldsymbol{J}_z^2\big) + \big(\boldsymbol{S}^2 - \boldsymbol{S}_z^2\big) + \big(\boldsymbol{L}_x^2 + \boldsymbol{L}_y^2\big) - (\boldsymbol{J}_+\boldsymbol{S}_- + \boldsymbol{J}_-\boldsymbol{S}_+) - (\boldsymbol{J}_+\boldsymbol{L}_- + \boldsymbol{J}_-\boldsymbol{L}_+) + (\boldsymbol{S}_+\boldsymbol{L}_- + \boldsymbol{S}_-\boldsymbol{L}_+)\big], \quad (1)$$

where r is the internuclear separation, and the standard designations for the molecular angular momenta are used. However, in the actual computations we only included the diagonal part (the three first parenthesis) and the S-uncoupling part (the fourth parenthesis) of this Hamiltonian, while the L-uncoupling and the homogeneous spin–electron parts (two last parenthesis) were ignored.

We also ignored all other interactions dealing with the rotational momentum $\boldsymbol{R}$ as well as the interactions between two electronic spins (spin-spin) and between two nuclear spins (nuclear spin-spin); this is justified for the states observed in the ultracold photoassociation of alkali metals, as they belong to the lowest rotational states and were located at large internuclear separations.

The effective interaction Hamiltonian was composed of four terms:

$$H^{\text{int}} = H^{SO} + H^{IL} + H^{IS} + H^{EQ}, \quad (2)$$

where

$$H^{SO} = \sum_i a_i(\boldsymbol{l}_i \cdot \boldsymbol{s}_i) \quad (3)$$

is the spin-orbit (SO) interaction,

$$H^{IS} = \sum_{i,k} b_{ik}(\boldsymbol{s}_i \cdot \boldsymbol{I}_k) \quad (4)$$

TABLE I. The atomic parameters (GHz) of the fine and hyperfine interactions in the designations of the present work.

	Na(s)	Cs(s)	Cs(p)
A	0	0	5536.5565501
$b_{\mathrm{Na,Cs}}$	0.4429065	1.1490790	− 0.09568497
$c_{\mathrm{Na,Cs}}$	0	0	0.08554940
$q_{\mathrm{Na,Cs}}$	0	0	− 0.0005096

is the interaction between the nuclear and electronic spins (IS),

$$H^{IL} = \sum_{i,k} c_{ik}(\boldsymbol{l}_i \cdot \boldsymbol{I}_k) \tag{5}$$

is the interaction between the nuclear spins and the electronic orbits (IL), and

$$H^{EQ} = \sum_{k} \boldsymbol{T}^2(\nabla \boldsymbol{E}_k) \cdot \boldsymbol{T}^2(\boldsymbol{Q}_k) \tag{6}$$

is the electric quadrupole interaction (EQ). Here k numerates the nuclei, i numerates the electrons, $\boldsymbol{I}_k$ is the spin of the kth nucleus, $\boldsymbol{s}_i$ is the spin of the ith electron, $\boldsymbol{l}_i$ is the orbital momentum of the ith electron, $\boldsymbol{T}^2(\boldsymbol{Q}_k)$ is the second-order irreducible tensor of the kth nucleus electric quadrupole moment, and $\boldsymbol{T}^2(\nabla \boldsymbol{E}_k)$ is the second-order irreducible tensor of the electric field gradient at the kth nucleus. The parameters of the interactions can be expressed via dynamic variables of electrons and nuclei [36]. We imply that the term H^{IS} comprises both the Fermi contact interaction and the average dipolar interaction. The matrix elements of these Hamiltonian terms in the Hund's case (a_β) basis along with their asymptotic (atomic) forms are listed in the Appendices.

IV. NUMERICAL SIMULATIONS

We suppose that the photoassociating atoms at the ground-state asymptote $s + s$ are initially at their lowest energetic states, i.e., they possess the atomic quantum numbers of the total momentum $f_{\mathrm{Na}} = 1$ and $f_{\mathrm{Cs}} = 3$. Depending on their mutual orientation in the s-wave scattering process, they are able to form molecular states with $F = 2, 3, 4$. In accordance with the selection rules, the photoassociation transitions are possible to the upper states with $F = 1, 2, 3, 4, 5$.

Therefore, at the ground-state asymptote we constructed the Hamiltonian matrices of H^{IS} for $F = 2, 3, 4$ using the asymptotic atomic parameters from Table I, in the full (a_β) basis of molecular states correlating with $s + s$. With the aim to restrict ourselves to only the s-wave scattering state, we projected these matrices onto the b_β basis with $N = 0$ with the help of the well-known transformation matrix [37]. We computed the eigenvectors of these matrices and chose those of them belonging to the lowest atomic hyperfine limit. Further on we supposed that these three states are incoherently mixed with weights $2F + 1$ in the unpolarized ensemble of the molecules; notice that when estimating the transition intensities via the squares of the reduced matrix elements of the electric dipole moment, the sum over all projections M_F is already taken into account; therefore there is no need to multiply these intensities by $2F + 1$.

Analogously, at the excited-state asymptote $s + p$ we constructed the Hamiltonian matrices for $F = 1, 2, 3, 4, 5$ using initially the asymptotic atomic parameters from Table I, in the full (a_β) basis of molecular states correlating with $s + p$. Positions of the four levels belonging to the unperturbed electronic states $^1\Sigma^+$, $^3\Sigma^+$, $^1\Pi$, and $^3\Pi$ varied (see below). In fact, this same model with the totally ignored rotation and all four levels with zero energies was explored to reproduce the asymptotic atomic structure and to determine the quantities in Table I.

The strong spin-orbit interaction splits all the eigenenergies into two largely separated groups. Further on we tracked the levels belonging to the upper $3s_{1/2} + 6p_{3/2}$ asymptote. The rotational constant $B_v \approx 0.485\,7$ GHz of the $c\,^3\Sigma_1^+$ state was estimated from intervals of the observed rotational levels of the $v = 61$ vibrational state. For the other (perturbing) states the rotation was ignored ($B_v = 0$).

Then we computed the matrix elements and the intensities of the electric dipole transitions between the three lower states and all the eigenvectors of the upper states. To compare the

TABLE II. Nonzero asymptotic matrix elements of the spin-orbit Hamiltonian term between molecular state vectors of an alkali-metal dimer at the $s + p$ asymptote (coefficients at the spin-orbit constant $A = (1/2)\langle p|a|p\rangle$).

	$^1\Sigma_0^+$	$^3\Sigma_0^+$	$^3\Pi_0(\Lambda=1)$	$^3\Pi_0(\Lambda=-1)$	$^3\Sigma_1^+$	$^1\Pi_1$	$^3\Pi_1$	$^3\Sigma_{-1}^+$	$^1\Pi_{-1}$	$^3\Pi_{-1}$	$^3\Pi_2$	$^3\Pi_{-2}$
$^1\Sigma_0^+$	0	0	−1	1								
$^3\Sigma_0^+$	0	0	1	1								
$^3\Pi_0(\Lambda=1)$	−1	1	−1	0								
$^3\Pi_0(\Lambda=-1)$	1	1	0	−1								
$^3\Sigma_1^+$					0	1	1					
$^1\Pi_1$					1	0	−1					
$^3\Pi_1$					1	−1	0					
$^3\Sigma_{-1}^+$								0	−1	1		
$^1\Pi_{-1}$								−1	0	1		
$^3\Pi_{-1}$								1	1	0		
$^3\Pi_2$											1	
$^3\Pi_{-2}$												1

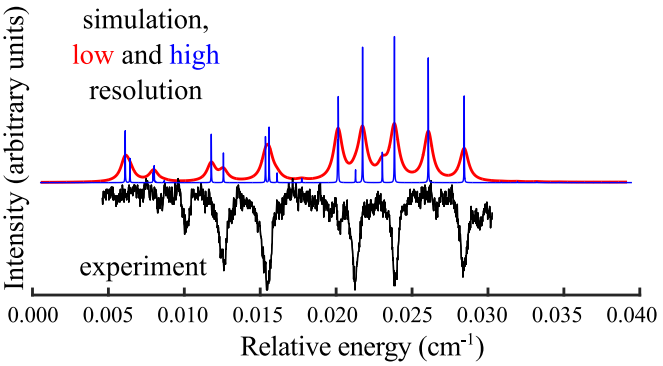

FIG. 4. The experimental loss spectrum of the NaCs $c\,^3\Sigma^+_{\Omega=1}$ ($v = 61, J = 1$) and its simulation with only energies of levels being varied.

spectrum with the experimental one, we approximated the lines by Lorentzians.

Initially we placed the levels of every electronic state into accidentally chosen different positions, separated by ~10 GHz. As soon as the spin-orbit interaction is turned on, the level of the $^3\Sigma^+$ state splits into the components $\Omega = 0$ and $\Omega = 1$ (more correctly, the blended states in accordance with Table II). To determine which one is which, we did a numerical experiment: the position of the component $\Omega = 1$ is highly sensitive to the moves of the levels of the Π states and weakly sensitive to the moves of the $^1\Sigma$ state, while the component $\Omega = 0$ is more sensitive to the moves of $^1\Sigma^+$ and weakly sensitive to the moves of $^1\Pi$ state levels (see Table II). As soon as all the other interactions are turned on, the hyperfine structure is revealed.

Certainly, within our model the line positions and intensities depend on the relative positions of the four unperturbed levels. We tried to adjust their positions in order to get a reasonable reproduction of the experimental spectrum. Our best result is compared to the experimental spectrum in Fig. 4. Note that in Figs. 4–7 below we use identical scales of both the axes.

The simulated spectrum has a definite resemblance of the experimental spectrum (the same overall spread, similar distribution of peaks), but the discrepancies are also evident. To improve the situation, we tried to vary the molecular interaction parameters along with the energies of the levels. The result is shown in Fig. 5, achieved with the (IS) molecular parameters being varied. The final values of the interaction parameters

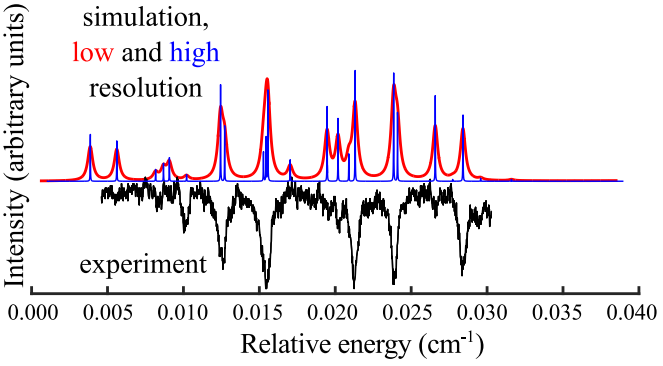

FIG. 5. The experimental loss spectrum of the NaCs $c\,^3\Sigma^+_{\Omega=1}$ ($v = 61, J = 1$) and its final simulation.

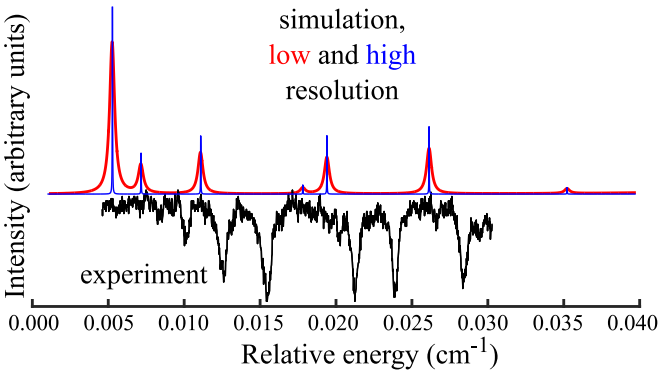

FIG. 6. The experimental loss spectrum of the NaCs $c\,^3\Sigma^+_{\Omega=1}$ ($v = 61, J = 1$) and its simulation with the (IS) interaction turned off.

differ from the asymptotic ones by ~10%. We were unable to find a better simulation than this one. An attempt to vary additionally the (IL) parameters and/or the rotational constants B_v did not result in a significant improvement, and even produced numerical instabilities.

In order to assess the role of different terms of the hyperfine Hamiltonian, we did the simulations with definite interactions being turned off. Figure 6 shows the result achieved without the (IS) interaction, and Fig. 7 shows the result achieved without the (IL) interaction. We see that both effects contribute significantly. Turning off the electric quadrupole interaction (EQ) hardly changed the simulated spectrum.

The spectra can be interpreted as combinations of the hyperfine structures of the electronic states blended at this level. This is clearly seen in Fig. 6, where the observed lines can be treated as two (IL) multiplets originating from the intermixes of the $^3\Pi_1$ and $^1\Pi_1$ states. (In accordance with $j = 3/2$, they must be tetraplets.)

The spectrum in Fig. 7 is more complicated, first of all because, contrary to the case of Fig. 6, both atoms contribute, and the (IS) interaction parameters were shifted from their asymptotic values. Supposedly, it represents the (IS) structure of two triplet intermixes to the $\Omega = 1$ state ($^3\Sigma^+_1$ and $^3\Pi_1$).

We would also like to emphasize that the assignment of the state as $^3\Sigma^+_1$ is no more than conventional. All three states with $\Omega = 1$ present with noticeable weights. Rather, it can be characterized as the Hund's case (c) state $\Omega = 1$.

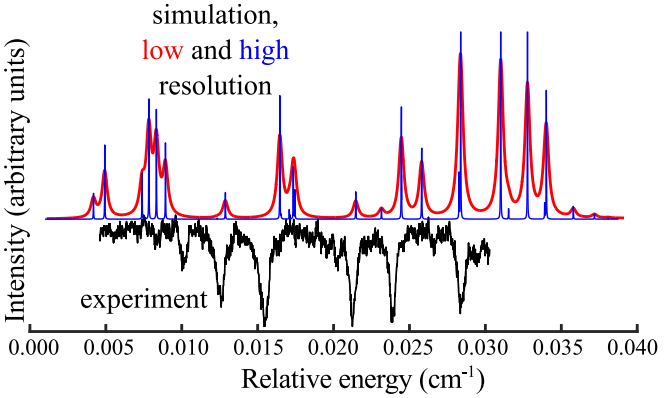

FIG. 7. The experimental loss spectrum of the NaCs $c\,^3\Sigma^+_{\Omega=1}$ ($v = 61, J = 1$) and its simulation with the (IL) interaction turned off.

V. DISCUSSION

For sure, the model being explored has many limitations. First, the interactions are in fact global and in general cannot be accurately described in terms of the local interactions between a few levels; see our work [20] where only the full-scale quantum mechanical multichannel computation was able to reproduce the rovibrational structure of the near-dissociation levels of Cs_2 at the asymptote $6S_{1/2} + 6P_{1/2}$. Such a computation would allow us to estimate accurately the PA strengths as well, but for a while this is out of the scope of the present work. In the present simulation our basis comprised several hundreds of states. In our experience, the mapped Fourier grid method [38–41] (employed in Ref. [20]) requires ∼100 or more nodes of the spatial grid. This leads to the Hamiltonian matrix of the size $\sim 10^5 \times 10^5$. The situation is somehow relaxed by the fact that this matrix is sparse, giving way to computational approaches developed for sparse matrices. Nevertheless, such a computation would require substantial computational resources, especially in a view of its use in a fitting procedure.

If even such a computation would be done, there are many other factors influencing the observations. Among them are: possible contributions from the scattering states higher than the s-wave state; possible presence of the atoms at the other f states than the lowest ones; possible polarization of the initial ensemble of atoms caused by the polarized radiation of the cooling lasers, which could be not totally thermalized; complicated mechanisms of the decay of the associated atoms; possible deviations from the Condon approximation; perturbations from the states of other atomic limits; and the interaction mechanisms currently ignored. The remaining discrepancies of the experimental and simulated spectra can indicate that some of those factors are significant.

Meanwhile, the present model is relatively simple and requires reasonable computational efforts. Of course, it can be hardly considered as being quantitative but rather illustrative. This is why we restricted its application to only one observed level. Nevertheless, this simple model is able to reproduce the overall characteristic hyperfine structure of the experimental spectra. The simulated spectrum in Fig. 5 has the same characteristic spread and intervals between peaks as the experimental one; the counterpartners can be found for all intense peaks. The model allows one to reveal physical mechanisms underlying the observed hyperfine structure and enables better understanding of near-dissociation properties.

VI. CONCLUSIONS

We have observed five near-dissociation rovibrational levels of the $c\,^3\Sigma^+$ electronic state of NaCs below the atomic limit $3S_{1/2} + 6P_{3/2}$. All the levels contain significant hyperfine structures. There are at least seven prominent hyperfine resonance peaks in each rovibrational level observed in the spectra. The simplified model of four vibrational levels belonging to different initially unperturbed electronic states is proposed to explain the hyperfine structure of alkali-metal dimers at the limit $s + p$. This model provided a reasonable reproduction of the experimental loss spectrum of the near-dissociation level in the $c\,^3\Sigma^+$ state. The hyperfine structure is mostly caused by the interactions of the nuclear spins with the electronic spins and with the electronic orbits. The interaction parameters are close to the asymptotic parameters of the pair of atoms. The coupling of the electronic states is essential for the interpretation of the hyperfine structure.

ACKNOWLEDGMENTS

This work was supported by the State Key Development Program for Basic Research of China (Grant No. 2012CB921603), the Changjiang Scholars and Innovative Research Team in the University of the Ministry of Education of China (Grant No. IRT13076), National Natural Science Foundation of China (Grants No. 91436108, No. 61378014, No. 61308023, No. 61378015, No. 11402140, No. 11404197, and No. 11434007), Scientific Research Fund for the Doctoral Program of Higher Education of China (Grant No. 20131401120012).

APPENDIX A: MATRIX ELEMENTS

Within the Hund's case (a_β) coupling scheme, the matrix elements of the Hamiltonian terms can be expressed via the quantum numbers of the basis states. Using the standard designations from the algebra of the quantum angular momentum [42] and from the molecular spectroscopy [43], the resulting expressions are as follows.

The diagonal part of the rotational Hamiltonian:

$$\begin{aligned}&\langle n\Lambda S\Sigma J\Omega I F M_F|B_v\left[\left(\boldsymbol{J}^2-\boldsymbol{J}_z^2\right)+\left(\boldsymbol{S}^2-\boldsymbol{S}_z^2\right)+\left(\boldsymbol{L}_x^2+\boldsymbol{L}_y^2\right)\right]|n'\Lambda'S'\Sigma'J'\Omega'I'FM_F\rangle\\&\quad=\delta_{\Lambda\Lambda'}\delta_{SS'}\delta_{JJ'}\delta_{\Omega\Omega'}\delta_{II'}B_v[J(J+1)-\Omega^2+S(S+1)-\Sigma^2+\epsilon],\end{aligned}\tag{A1}$$

where ϵ is a small contribution from the last parenthesis of this part, which is usually ignored or attributed to the adiabatic potential function (or vibrational energy for the isolated level).

The S-uncoupling term of the rotational Hamiltonian:

$$\begin{aligned}&\langle n\Lambda S\Sigma J\Omega I F M_F|-\frac{\hbar^2}{2mr^2}(\boldsymbol{J}_+\boldsymbol{S}_-+\boldsymbol{J}_-\boldsymbol{S}_+)|n'\Lambda'S'\Sigma'J'\Omega'I'F'M_F\rangle\\&\quad=-\delta_{nn'}\delta_{\Lambda\Lambda'}\delta_{II'}\delta_{FF'}\delta_{JJ'}\delta_{SS'}\langle n\Lambda|\frac{\hbar^2}{2mr^2}|n\Lambda\rangle[\{[J(J+1)-\Omega'(\Omega'-1)][S(S+1)-\Sigma'(\Sigma'-1)]\}^{1/2}\delta_{\Omega,\Omega'-1}\\&\qquad+\{[J(J+1)-\Omega'(\Omega'+1)][S(S+1)-\Sigma'(\Sigma'+1)]\}^{1/2}\delta_{\Omega,\Omega'+1}].\end{aligned}\tag{A2}$$

The spin-orbit interaction:

$$\langle n\Lambda S\Sigma J\Omega I F M_F|H^{SO}|n'\Lambda' S'\Sigma' J'\Omega' I' F M_F\rangle = \delta_{II'}\delta_{JJ'}\delta_{\Omega\Omega'}(-1)^{\Lambda-\Lambda'+S-\Sigma}\begin{pmatrix} S & 1 & S' \\ -\Sigma & (\Lambda'-\Lambda) & \Sigma' \end{pmatrix}\mathcal{A}, \tag{A3}$$

where

$$\mathcal{A} = \sum_i \langle n\Lambda|a_i \tilde{\boldsymbol{T}}^1_{\Lambda-\Lambda'}(\boldsymbol{l}_i)|n'\Lambda'\rangle\langle S\|\tilde{\boldsymbol{T}}^1(\boldsymbol{s}_i)\|S'\rangle, \tag{A4}$$

and $\tilde{\boldsymbol{T}}^k_q$ designates the qth component of the irreducible tensor operator in the molecule–fixed coordinate system, while $\boldsymbol{T}^k_q$ relates the space–fixed coordinate system.

The nuclear spin–electronic spin interaction:

$$\begin{aligned}
&\langle n\Lambda S\Sigma J\Omega I F M_F|H^{IS}|n'\Lambda' S'\Sigma' J'\Omega' I' F M_F\rangle \\
&= (-1)^{F-S+I+I'+I_1+I_2-\Lambda}\delta_{\Lambda\Lambda'}[(2J+1)(2J'+1)(2I+1)(2I'+1)]^{1/2}\begin{Bmatrix} J & I & F \\ I' & J' & 1 \end{Bmatrix}\begin{pmatrix} J & 1 & J' \\ \Omega & (\Omega'-\Omega) & -\Omega' \end{pmatrix} \\
&\times\begin{pmatrix} S & 1 & S' \\ -\Sigma & (\Sigma-\Sigma') & \Sigma' \end{pmatrix}\sum_{k=1}^{2}[(2I_k+1)I_k(I_k+1)]^{1/2}\left[\delta_{k1}\begin{Bmatrix} I' & I & 1 \\ I_1 & I_1 & I_2 \end{Bmatrix} + \delta_{k2}(-1)^{I-I'}\begin{Bmatrix} I' & I & 1 \\ I_2 & I_2 & I_1 \end{Bmatrix}\right]\mathcal{B}_k,
\end{aligned} \tag{A5}$$

where

$$\mathcal{B}_k = \sum_i \langle n\Lambda|b_{ik}|n'\Lambda\rangle\langle S\|\tilde{\boldsymbol{T}}^1(\boldsymbol{s}_i)\|S'\rangle. \tag{A6}$$

The nuclear spin–electronic orbit interaction:

$$\begin{aligned}
&\langle n\Lambda S\Sigma J\Omega I F M_F|H^{IL}|n'\Lambda' S'\Sigma' J'\Omega' I' F M_F\rangle \\
&= \delta_{SS'}\delta_{\Sigma\Sigma'}(-1)^{F+I+I'+I_1+I_2-\Omega}[(2J+1)(2J'+1)(2I+1)(2I'+1)]^{1/2}\begin{pmatrix} J & 1 & J' \\ \Omega & (\Omega'-\Omega) & -\Omega' \end{pmatrix}\begin{Bmatrix} F & J' & I' \\ 1 & I & J \end{Bmatrix} \\
&\times\sum_{k=1}^{2}[(2I_k+1)I_k(I_k+1)]^{1/2}\left[\delta_{k1}\begin{Bmatrix} I_1 & I & I_2 \\ I' & I_1 & 1 \end{Bmatrix} + \delta_{k2}(-1)^{I-I'}\begin{Bmatrix} I_2 & I & I_1 \\ I' & I_2 & 1 \end{Bmatrix}\right]\mathcal{C}_k,
\end{aligned} \tag{A7}$$

where

$$\mathcal{C}_k = \sum_i \langle n\Lambda|c_{ik}\tilde{\boldsymbol{T}}^1_{\Lambda-\Lambda'}(\boldsymbol{l}_i)|n'\Lambda'\rangle. \tag{A8}$$

The electric quadrupole interaction:

$$\begin{aligned}
&\langle n\Lambda S\Sigma J\Omega I F M_F|H^{EQ}|n'\Lambda' S'\Sigma' J'\Omega' I' F M_F\rangle \\
&= (-1)^{F-\Omega+I+I'+I_1+I_2}\delta_{SS'}\delta_{\Sigma\Sigma'}[(2J+1)(2J'+1)(2I+1)(2I'+1)]^{1/2} \\
&\times\begin{pmatrix} J & 2 & J' \\ \Omega & (\Lambda'-\Lambda) & -\Omega' \end{pmatrix}\begin{Bmatrix} F & J & I \\ 2 & I' & J' \end{Bmatrix}\left[\begin{Bmatrix} I_1 & I & I_2 \\ I' & I_1 & 2 \end{Bmatrix}\mathcal{Q}_1 + (-1)^{(I-I')}\begin{Bmatrix} I_2 & I & I_1 \\ I' & I_2 & 2 \end{Bmatrix}\mathcal{Q}_2\right]
\end{aligned} \tag{A9}$$

with

$$\mathcal{Q}_k = \langle n\Lambda|\tilde{\boldsymbol{T}}^2_{\Lambda-\Lambda'}(\nabla\boldsymbol{E}_k)|n'\Lambda'\rangle\langle I_k\|\boldsymbol{T}^2(\boldsymbol{Q}_k)\|I_k\rangle. \tag{A10}$$

The common convention is to introduce the scalar quadrupole moment of a nucleus:

$$Q(k) \equiv \langle I_k, M_{I_k} = I_k|\sum_{\text{nuclons}\,p}\left(3z_p^2 - r_p^2\right)|I_k, M_{I_k} = I_k\rangle \tag{A11}$$

and

$$q(k) \equiv 2\langle n\Lambda|\tilde{\boldsymbol{T}}^2_{\Lambda-\Lambda'}(\nabla\boldsymbol{E}_k)|n'\Lambda'\rangle, \tag{A12}$$

so that

$$\mathcal{Q}_k = \frac{1}{4}eQ(k)q(k)\left[\frac{(2I_k+3)(2I_k+2)(2I_k+1)}{2I_k(2I_k-1)}\right]^{1/2}. \tag{A13}$$

However, throughout the work we used the values $\mathcal{Q}_k$ but not $eQ(k)q(k)$ as the parameters of the electric quadrupole interaction.

To complete the computations, we also need the (reduced) matrix element of the electric dipole transition operator in the Hund's case (a_β) basis. Here it is:

$$\langle n\Lambda S\Sigma J\Omega I F\|\boldsymbol{T}^1(\boldsymbol{d})\|n'\Lambda' S'\Sigma' J'\Omega' I' F'\rangle = \delta_{SS'}\delta_{\Sigma\Sigma'}\delta_{II'}(-1)^{F'+I+\Omega+1}[(2F+1)(2F'+1)(2J+1)(2J'+1)]^{1/2} \times\begin{pmatrix} J' & 1 & J \\ -\Omega' & (\Omega'-\Omega) & \Omega\end{pmatrix}\begin{Bmatrix} J & F & I \\ F' & J' & 1\end{Bmatrix}\mathcal{M}, \tag{A14}$$

where

$$\mathcal{M} = \langle n\Lambda|\tilde{\boldsymbol{T}}^1_{\Lambda-\Lambda'}(\boldsymbol{d})|n'\Lambda'\rangle, \tag{A15}$$

and $\boldsymbol{d}$ is the electric dipole of the electrons. Within the present work we supposed $\mathcal{M} = \text{const}$ (Condon approximation).

APPENDIX B: ATOMIC ASYMPTOTE

At the asymptote of large internuclear separations, all the molecular equations must reproduce the energetic structure of two independent atoms.

At the ground-state asymptote $s+s$ ($\Lambda=\Lambda'=0$, $S,S'=0,1$), the only nonzero interaction matrix element is the one of Eq. (A5), arising from the Fermi contact interaction at the atoms. At the asymptote $s+p$ ($\Lambda,\Lambda'=0,1$, $S,S'=0,1$), all four terms contribute.

Addressing the properly symmetrized asymptotic atomic configuration functions of the two-electron systems of alkali-metal dimers,

$$|n^1\Lambda\rangle \to \frac{1}{\sqrt{2}}[\psi_1(\boldsymbol{q}_1)\psi_2(\boldsymbol{q}_2)+\psi_1(\boldsymbol{q}_2)\psi_2(\boldsymbol{q}_1)], \quad |n^3\Lambda\rangle \to \frac{1}{\sqrt{2}}[\psi_1(\boldsymbol{q}_1)\psi_2(\boldsymbol{q}_2)-\psi_1(\boldsymbol{q}_2)\psi_2(\boldsymbol{q}_1)], \tag{B1}$$

where $\psi_k(\boldsymbol{q}_i)$ is the state function of the kth atom at the position $\boldsymbol{q}_i$ of the ith electron, we get for the electronic matrix elements of some operator $\boldsymbol{h}_{ik}$:

$$\begin{aligned}
\langle n\,^1\Lambda|\boldsymbol{h}_{ik}|n'\,^1\Lambda'\rangle &\to \frac{1}{2}\delta_{\psi_{\tilde{k}},\psi'_{\tilde{k}}}\langle\psi_k(\boldsymbol{q}_k)|\boldsymbol{h}_{kk}|\psi'_k(\boldsymbol{q}_k)\rangle,\\
\langle n\,^3\Lambda|\boldsymbol{h}_{ik}|n'\,^3\Lambda'\rangle &\to \frac{1}{2}\delta_{\psi_{\tilde{k}},\psi'_{\tilde{k}}}\langle\psi_k(\boldsymbol{q}_k)|\boldsymbol{h}_{kk}|\psi'_k(\boldsymbol{q}_k)\rangle,\\
\langle n\,^1\Lambda|\boldsymbol{h}_{ik}|n'\,^3\Lambda'\rangle &\to \frac{(-1)^{(k+i)}}{2}\delta_{\psi_{\tilde{k}},\psi'_{\tilde{k}}}\langle\psi_k(\boldsymbol{q}_k)|\boldsymbol{h}_{kk}|\psi'_k(\boldsymbol{q}_k)\rangle,
\end{aligned} \tag{B2}$$

where $\psi_{\tilde{k}}$ is the wave function of the other (not kth) atom. Besides,

$$\begin{aligned}
\langle(1/2,1/2)S\|\boldsymbol{T}^1(\boldsymbol{s}_i)\|(1/2,1/2)S'\rangle &= (-1)^{S'(2-i)+S(i-1)}[(2S+1)(2S'+1)]^{1/2}\begin{Bmatrix}\frac{1}{2} & S & \frac{1}{2}\\ S' & \frac{1}{2} & 1\end{Bmatrix}\sqrt{\frac{3}{2}}\\
&= \begin{cases} 0, & S=S'=0\\ \sqrt{3/2}, & S=S'=1\\ (-1)^i\sqrt{3}/2, & S=0,\ S'=1\\ (-1)^{i-1}\sqrt{3}/2, & S=1,\ S'=0\end{cases}, \quad i=1,2.
\end{aligned} \tag{B3}$$

These properties give way to deduce the asymptotic molecular matrix elements in terms of the atomic matrix elements.

In part [see Eq. (A6) for $\mathcal{B}_k$],

$$\begin{aligned}
\sum_i\langle^3\Lambda|b_{ik}|^3\Lambda\rangle\langle S=1\|\boldsymbol{T}^1(\boldsymbol{s}_i)\|S'=1\rangle &\to \sqrt{6}\,b_k,\\
\sum_i\langle^3\Lambda|b_{ik}|^1\Lambda\rangle\langle S=1\|\boldsymbol{T}^1(\boldsymbol{s}_i)\|S'=0\rangle &= -\sum_i\langle^1\Lambda|b_{ik}|^3\Lambda\rangle\langle S=0\|\boldsymbol{T}^1(\boldsymbol{s}_i)\|S'=1\rangle\\
&\to (-1)^{k-1}\sqrt{3}\,b_k,
\end{aligned} \tag{B4}$$

with

$$b_k = \tfrac{1}{2}\langle nl|b_{kk}|nl\rangle \tag{B5}$$

being half of the kth atom diagonal electronic matrix element.

Then [see Eq. (A8) for $\mathcal{C}_k$]

$$\langle n\Lambda|\sum_{i=1}^{2} c_{ik}\boldsymbol{T}^1_q(\boldsymbol{l}^{(i)})|n'\Lambda'\rangle = \sum_{i=1}^{2}\frac{1}{2}\langle\psi_k|c_{kk}\boldsymbol{T}^1_q(\boldsymbol{l}_k)|\psi'_k\rangle = \frac{1}{2}\sum_{i=1}^{2}\langle n_k l_k|c_{kk}|n'_k l'_k\rangle\langle l_k m_{l_k}|\boldsymbol{T}^1_q(\boldsymbol{l}_k)|l'_k m_{l'_k}\rangle$$
$$= (-1)^{l_k-m_{l_k}}2\begin{pmatrix} l_k & 1 & l_k \\ -m_{l_k} & q & m'_{l_k}\end{pmatrix}[(2l_k+1)l_k(l_k+1)]^{1/2}\delta_{l_k l'_k}\left[\frac{1}{2}\langle n_k l_k|c_{kk}|n'_k l'_k\rangle\right], \tag{B6}$$

or, for the case of the $s+p$ limit ($l_1=0, l_2=1, m_{l_2}=\Lambda$),

$$\langle n\Lambda|\sum_{i=1}^{2} c_{ik}\boldsymbol{T}^1_q(\boldsymbol{l}^{(i)})|n'\Lambda'\rangle = \delta_{k2}2\sqrt{6}(-1)^{\Lambda-1}\begin{pmatrix} 1 & 1 & 1 \\ -\Lambda & q & \Lambda'\end{pmatrix}c_2 \tag{B7}$$

with

$$c_2 = \tfrac{1}{2}\langle np|c_{2,2}|np\rangle. \tag{B8}$$

Then [see Eq. (B9) for $\mathcal{Q}_k$], at the asymptote $s+p$,

$$\langle n\Lambda|\tilde{\boldsymbol{T}}^2_{\Lambda-\Lambda'}(\nabla\boldsymbol{E}_k)|n'\Lambda'\rangle\langle I_k\|\boldsymbol{T}^2(\boldsymbol{Q}_k)\|I_k\rangle \to \delta_{k2}(-1)^{\Lambda-1}\begin{pmatrix} 1 & 2 & 1 \\ -\Lambda & (\Lambda-\Lambda') & \Lambda'\end{pmatrix}\sqrt{30}\,q_2, \tag{B9}$$

where

$$q_2 = \langle p_1|\boldsymbol{T}^2_0(\nabla\boldsymbol{E}_2)|p_1\rangle\langle I_2\|\boldsymbol{T}^2(\boldsymbol{Q}_2)\|I_2\rangle, \tag{B10}$$

and p_1 designates the atomic state with the orbital momentum equal to 1 and its projection equal to 1.

Analogous to Ref. [44], the asymptotic matrix elements of the spin-orbit interaction at the limit $s+p$ are presented in Table II in the form of coefficients at the spin-orbit constant $A=(1/2)\langle p|a_2|p\rangle$. There are two differences between our table and the table in [44]. First, the signs of all the matrix elements between the states of different multiplicities are opposite; this could occur due to the different order of coupling of the two atoms into a molecule. Second, we have not split the matrix $\Omega=0$ into two independent matrices with definite reflection parities "±"; we prefer using the initial basis because with it all the matrix elements are easier expressed and manipulated. Both differences are purely technical and cannot lead to a difference for anything observable.

We have determined the atomic parameters, expressed in the designations of the present work, by fitting our asymptotic molecular equations to the term values of the atomic pair Na + Cs. The experimental term values of the atoms were taken from Refs. [45–52]. The results are listed in Table I. The residuals of the reproduction of the atomic pair term values with these parameters are $\sim 2\times10^{-3}$ MHz.

It is also seen from Eqs. (B3) that for any transition between molecular states of the asymptotes $s+s$ and $s+p$, the transition matrix elements Eq. (A15) are just a sum of the corresponding atomic matrix elements, one of which [Na(s) → Na(s)] is always zero. The pure rotation approximation is valid at both asymptotes. Applying the Wigner-Eckart theorem [42] we have

$$\langle n,L=0,\Lambda=0|\tilde{\boldsymbol{T}}^1_{-\Lambda'}(\boldsymbol{d})|n',L'=1,\Lambda'\rangle = \begin{pmatrix} 0 & 1 & 1 \\ 0 & -\Lambda' & \Lambda'\end{pmatrix}\langle n,L=0\|\tilde{\boldsymbol{T}}^1(\boldsymbol{d})\|n',L'=1\rangle$$
$$= (-1)^{1-\Lambda'}\frac{1}{\sqrt{3}}\langle n,L=0\|\tilde{\boldsymbol{T}}^1(\boldsymbol{d})\|n',L'=1\rangle. \tag{B11}$$

Therefore the transition matrix elements change signs for transitions to the states with different Λ'; up to this change of sign the Condon approximation is justified asymptotically.

[1] J. Ulmanis, J. Deiglmayr, M. Repp, R. Wester, and M. Weidemüller, Chem. Rev. (Washington, DC, U. S.) **112**, 4890 (2012).

[2] D. S. Jin and J. Ye, Chem. Rev. (Washington, DC, U. S.) **112**, 4801 (2012).

[3] G. Quéméner and P. S. Julienne, Chem. Rev. (Washington, DC, U. S.) **112**, 4949 (2012).

[4] J. Kleinert, C. Haimberger, P. J. Zabawa, and N. P. Bigelow, Phys. Rev. Lett. **99**, 143002 (2007).

[5] S. Ospelkaus, K.-K. Ni, D. Wang, M. H. G. de Miranda, B. Neyenhuis, G. Quéméner, P. S. Julienne, J. L. Bohn, D. S. Jin, and J. Ye, Science **327**, 853 (2010).

[6] R. V. Krems, Phys. Chem. Chem. Phys. **10**, 4079 (2008).

[7] V. V. Flambaum and M. G. Kozlov, Phys. Rev. Lett. **99**, 150801 (2007).

[8] T. A. Isaev, S. Hoekstra, and R. Berger, Phys. Rev. A **82**, 052521 (2010).

[9] J. J. Hudson, D. M. Kara, I. J. Smallman, B. E. Sauer, M. Tarbutt, and E. A. Hinds, Nature (London) **473**, 493 (2011).

[10] D. DeMille, Phys. Rev. Lett. **88**, 067901 (2002).

[11] L. Santos, G. V. Shlyapnikov, P. Zoller, and M. Lewenstein, Phys. Rev. Lett. **85**, 1791 (2000).

[12] M. A. Baranov, M. Dalmonte, G. Pupillo, and P. Zoller, Chem. Rev. (Washington, DC, U. S.) **112**, 5012 (2012).

[13] M. Schnell and G. Meijer, Angew. Chem., Int. Ed. **48**, 6010 (2009).
[14] J. Deiglmayr, A. Grochola, M. Repp, K. Mörtlbauer, C. Glück, J. Lange, O. Dulieu, R. Wester, and M. Weidemüller, Phys. Rev. Lett. **101**, 133004 (2008).
[15] S. Dutta, J. Lorenz, A. Altaf, D. S. Elliott, and Y. P. Chen, Phys. Rev. A **89**, 020702(R) (2014).
[16] D. Wang, J. Qi, M. F. Stone, O. Nikolayeva, H. Wang, B. Hattaway, S. D. Gensemer, P. L. Gould, E. E. Eyler, and W. C. Stwalley, Phys. Rev. Lett. **93**, 243005 (2004).
[17] A. J. Kerman, J. M. Sage, S. Sainis, T. Bergeman, and D. DeMille, Phys. Rev. Lett. **92**, 033004 (2004).
[18] A. Ridinger, S. Chaudhuri, T. Salez, D. R. Fernandes, N. Bouloufa, O. Dulieu, C. Salomon, and F. Chevy, Europhys. Lett. **96**, 33001 (2011).
[19] K. Aikawa, D. Akamatsu, M. Hayashi, K. Oasa, J. Kobayashi, P. Naidon, T. Kishimoto, M. Ueda, and S. Inouye, Phys. Rev. Lett. **105**, 203001 (2010).
[20] W. Liu, R. Xu, J. Wu, J. Yang, S. S. Lukashov, V. B. Sovkov, X. Dai, J. Ma, L. Xiao, and S. Jia, J. Chem. Phys. **143**, 124307 (2015).
[21] J. Kim, S. Moal, M. Portier, J. Dugué, M. Leduc, and C. Cohen-Tannoudji, Europhys. Lett. **72**, 548 (2005).
[22] D. DeMille, S. Sainis, J. Sage, T. Bergeman, S. Kotochigova, and E. Tiesinga, Phys. Rev. Lett. **100**, 043202 (2008).
[23] M. Aymar and O. Dulieu, J. Chem. Phys. **122**, 204302 (2005).
[24] P. Zabawa, A. Wakim, M. Haruza, and N. P. Bigelow, Phys. Rev. A **84**, 061401(R) (2011).
[25] C. Haimberger, J. Kleinert, M. Bhattacharya, and N. P. Bigelow, Phys. Rev. A **70**, 021402(R) (2004).
[26] A. Grochola, P. Kowalczyk, J. Szczepkowski, W. Jastrzebski, A. Wakim, P. Zabawa, and N. P. Bigelow, Phys. Rev. A **84**, 012507 (2011).
[27] A. Wakim, P. Zabawa, and N. P. Bigelow, Phys. Chem. Chem. Phys. **13**, 18887 (2011).
[28] A. Wakim, P. Zabawa, M. Haruza, and N. P. Bigelow, Opt. Express **20**, 16083 (2012).
[29] E. Tiesinga, K. M. Jones, P. D. Lett, U. Volz, C. J. Williams, and P. S. Julienne, Phys. Rev. A **71**, 052703 (2005).
[30] D. Comparat, C. Drag, A. Fioretti, O. Dulieu, and P. Pillet, J. Mol. Spectrosc. **195**, 229 (1999).
[31] K. M. Jones, E. Tiesinga, P. D. Lett, and P. S. Julienne, Rev. Mod. Phys. **78**, 483 (2006).
[32] H. Wang and W. C. Stwalley, J. Chem. Phys. **108**, 5767 (1998).
[33] J. Ma, L. R. Wang, Y. T. Zhao, L. T. Xiao, and S. T. Jia, J. Mol. Spectrosc. **255**, 106 (2009).
[34] J. P. Shaffer, W. Chalupczak, and N. P. Bigelow, Phys. Rev. A **60**, R3365 (1999).
[35] P. J. Zabawa, Ph.D. thesis, University of Rochester, 2012.
[36] J. M. Brown and A. Carrington, *Rotational Spectroscopy of Diatomic Molecules*, edited by R. J. Saykally, A. H. Zewail, and D. A. King (Cambridge University Press, Cambridge, UK, 2003).
[37] J. M. Brown and B. J. Howard, Mol. Phys. **31**, 1517 (1976).
[38] C. C. Martson and G. G. Balint-Kurti, J. Chem. Phys. **91**, 3571 (1989).
[39] V. Kokoouline, O. Dulieu, R. Kosloff, and F. Masnou-Seeuws, J. Chem. Phys. **110**, 9865 (1999).
[40] D. Lemoine, Chem. Phys. Lett. **320**, 492 (2000).
[41] K. Willner, O. Dulieu, and F. Masnou-Seeuws, J. Chem. Phys. **120**, 548 (2004).
[42] R. N. Zare, *Angular Momentum: Understanding Spatial Aspects in Chemistry and Physics* (John Wiley & Sons, New York, 1988).
[43] H. Lefebvre-Brion and R. W. Field, *The Spectra and Dynamics of Diatomic Molecules* (Elsevier, Academic Press, Amsterdam, 2004).
[44] A. Orbán, R. Vexiau, O. Krieglsteiner, H.-C. Nägerl, O. Dulieu, A. Crubellier, and N. Bouloufa-Maafa, Phys. Rev. A **92**, 032510 (2015).
[45] D. A. Steck, (2000; 2010), available online at http://steck.us/alkalidata (revision 2.1.4, 23 December 2010).
[46] D. A. Steck, (1998; 2010), available online at http://steck.us/alkalidata (revision 2.1.4, 23 December 2010).
[47] E. Arimondo, M. Inguscio, and P. Violino, Rev. Mod. Phys. **49**, 31 (1977).
[48] W. Yei, A. Sieradzan, and M. D. Havey, Phys. Rev. A **48**, 1909 (1993).
[49] W. A. van Wijngaarden and J. Li, Z. Phys. D: At., Mol. Clusters **32**, 67 (1994).
[50] T. Udem, J. Reichert, R. Holzwarth, and T. W. Hänsch, Phys. Rev. Lett. **82**, 3568 (1999).
[51] V. Gerginov, A. Derevianko, and C. E. Tanner, Phys. Rev. Lett. **91**, 072501 (2003).
[52] R. J. Rafac and C. E. Tanner, Phys. Rev. A **56**, 1027 (1997).